The growth and characterization of rhenium-doped WS_2 single crystals

2004 J. Phys.: Condens. Matter 16 2171

(http://iopscience.iop.org/0953-8984/16/12/025)

INSTITUTE OF PHYSICS PUBLISHING JOURNAL OF PHYSICS: CONDENSED MATTER

J. Phys.: Condens. Matter **16** (2004) 2171–2180 PII: S0953-8984(04)75114-0

The growth and characterization of rhenium-doped WS_2 single crystals

P C Yen[1], Y S Huang[1,3] and K K Tiong[2]

[1] Department of Electronic Engineering, National Taiwan University of Science and Technology, Taipei 106, Taiwan
[2] Department of Electrical Engineering, National Taiwan Ocean University, Keelung 202, Taiwan

Received 19 January 2004
Published 12 March 2004
Online at stacks.iop.org/JPhysCM/16/2171 (DOI: 10.1088/0953-8984/16/12/025)

Abstract

Single crystals of rhenium-doped WS_2 have been grown by the chemical vapour transport method using bromine as a transporting agent. From x-ray diffraction pattern analysis, the doped crystals are found to crystallize in mixed polytypes of the three-layer rhombohedral (3R) and two-layer hexagonal (2H) structures while the undoped one is in the 2H form. The x-ray photoelectron spectra (XPS) in the vicinity of W 5p core-level regime exhibit strongly asymmetric line-shape character and the weak shoulder located at higher energy side is attributed to the presence of a small amount of rhenium in WS_2. Hall coefficient measurements at room temperature indicate that the samples are n-type in nature. The doping effects of the materials are characterized by temperature-dependent conductivity, room temperature optical absorption and piezoreflectance (PzR) measurements. The drastic decrease in resistivity with increasing doping concentration suggests that more charge carriers are available for conduction in the doped compounds. The indirect energy gap for the doped samples shows red shifts on increasing the doping concentration. The direct band edge excitonic transition energies show a slight red shift due to the presence of a small amount of Re and the broadening parameter of the excitonic transition features increases due to impurity scattering.

1. Introduction

Layered-structure transition metal dichalcogenides MX_2 (M = W or Mo; X = Se or S) have been extensively investigated for their photovoltaic [1–4] and lubricating properties [5, 6]. WS_2 has been the subject of great interest, because its band gap is well matched to the solar spectrum [7]. It can act as an efficient photoconductive layer in photovoltaic devices and photoelectrochemical solar cells. The main advantage of WS_2 is the prevention of photo-corrosion, because the phototransitions involve nonbonding d–d orbitals of W atoms [8]. The

[3] Author to whom any correspondence should be addressed.

layered structure imparts a strong anisotropy in both mechanical and electrical properties. The anisotropy of the material is a result of the sandwich interlayer structure, loosely bonded by the weak van der Waals forces. The intralayer bonding is thought to be partly ionic and partly covalent, with the latter being dominant. There are two known polytypes of WS_2: two-layer hexagonal and three-layer rhombohedral, termed 2H and 3R, respectively [9, 10]. Both polytypes have regular layered structures with sixfold trigonal prismatic coordination of W atoms by the sulfur atoms within the layers. 2H-WS_2 has two layers per unit cell stacked in hexagonal symmetry and belongs to the space group D^4_{6h}, while 3R-WS_2 has rhombohedral symmetry with three layers along the *c*-axis and belongs to the space group C^5_{3v}. Earlier studies [11] suggested that natural rhombohedral MX_2 is consistently rich in certain minor elements (e.g. Re, Nb, Ti, Zr, Fe), and that the incorporation of such impurity elements has predetermined the adoption of the lower structural symmetry of MX_2, i.e. 3R. However, only few works concerning the effect of the dopants on the physical properties of WS_2 have been reported.

In this paper we report the growth and characterization of rhenium-doped WS_2 single crystals. Single crystals of WS_2 doped with Re were grown by the chemical vapour transport method using bromine as a transporting agent. The crystal structure was analysed using x-ray diffraction (XRD) patterns. The rhenium contents were examined by Auger electron spectroscopy (AES), energy-dispersive x-ray (EDX) analysis, and x-ray photoelectron spectroscopy (XPS). The temperature-dependent electrical conductivity measurements were carried out in the temperature range from 10 to 500 K. The indirect band-edge transitions and direct band-edge excitonic transitions were studied by transmittance and piezoreflectance (PzR), respectively. The effects of dopant (Re) on the electrical transport and optical properties are analysed and discussed.

2. Crystal growth

Single crystals of the system $W_{1-x}Re_xS_2$ were grown using the chemical vapour transport method with Br_2 as a transport agent. The total charge used in each growth experiment was about 10 g. The stoichiometrically determined weight of doping material (rhenium) was added in the hope that it would be transported at a rate similar to that of tungsten. Prior to the crystal growth, thermal treatment of the quartz ampoule (22 mm OD, 17 mm ID, 20 cm length) under vacuum must be performed to avoid any contamination from the quartz container. The quartz ampoule containing Br_2 ($\sim$5 mg cm^{-3}) and the elements (W, 99.99% pure; Re, 99.99%; S, 99.999%) was then cooled with liquid nitrogen, evacuated to 10^{-6} Torr and sealed. It was shaken well to obtain a uniform mixing of the powder. The ampoule was placed in a three-zone furnace and the charge prereacted for 24 h at 850 °C with the growth zone at 1000 °C, preventing the transport of the product. The temperature of the furnace was increased slowly. The slow heating was necessary to avoid any possibility of explosion due to the exothermic reaction between the elements. The furnace was then equilibrated to give a constant temperature across the reaction tube, and was programmed over 24 h to produce the temperature gradient at which single-crystal growth took place. Optimal results were obtained with a temperature gradient of approximately 1000 °C $\rightarrow$ 950 °C. After 240 h, the furnace was allowed to cool down slowly (40 °C h^{-1}) to about 200 °C. The ampoule was then removed and wet tissues applied rapidly to the end away from the crystals to condense the bromine vapour. When the ampoule reached room temperature, it was opened and the crystals were removed. The crystals were then rinsed with acetone and deionized water. Single crystalline platelets up to 8 $\times$ 8 mm^2 surface area and 1 mm in thickness were obtained. WS_2 crystallizes with 2H or 3R structure [12], while ReS_2 crystallizes in a distorted C6 structure [12, 13], so that only a small solubility range is

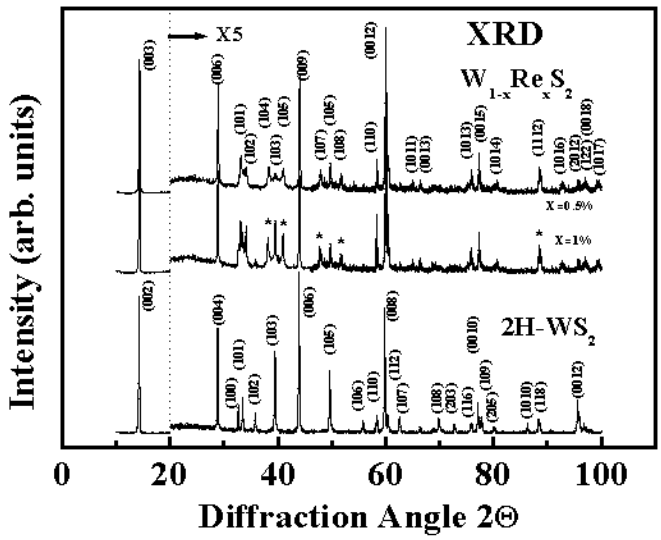

Figure 1. X-ray diffraction patterns of Re-doped WS_2 with $x = 0.5\%$, 1% and undoped WS_2. The additional lines (marked by *) were attributed to the presence of the rhombohedral polytype (3R).

to be expected. From our various growth attempts, we found that growing samples with large Re concentration was very difficult, due most likely to kinetic problems. In fact it was found that a nominal 5% Re doping of WS_2 prevented the growth of single crystals.

AES and EDX analysis were utilized to examine the contents of the Re composition x. The AES detection limits ($\sim$0.1%) can vary appreciably from element to element and be influenced by the beam current and analysis time, making quantitative AES analysis difficult [14]. Nevertheless, AES indicates the presence of a small quantity of Re, and the average concentration of Re in the sample crystals tends to vary from crystal to crystal. The EDX analysis is sensitive to concentration of $x \geqslant 0.01$ [14]. However, since no Re was detected by the EDX analysis, we conclude that the concentration of Re in the WS_2 crystals must be very low. The two transition metals (Re and W) are most probably chemically transported at different rates, and most of the doping material must remain in the untransported residual charge. A considerable discrepancy exists between the nominal doping ratios and those determined by means of AES and EDX. The actual concentration x is much lower than the intended one. Because of the immiscibility of the WS_2 and ReS_2, the formation of the ternary system $W_{1-x}Re_xS_2$ is not very likely, and the name is used only symbolically to represent the intended amount of Re in the growth of doped WS_2.

3. Characterization

3.1. X-ray diffraction

The crystal structure of $W_{1-x}Re_xS_2$ samples was analysed using a Rigaku RTP300RC x-ray diffractometer with Cu Kα radiation ($\lambda = 1.5418$ Å). For x-ray studies, several small crystals from batches of $W_{1-x}Re_xS_2$ with nominal (intended) concentration $x = 0.5\%$ and 1% were finely ground with a mixture of glass powder, and the x-ray powder patterns were recorded by means of a slow-moving radiation. Cu Kα radiation was employed and a silicon standard was

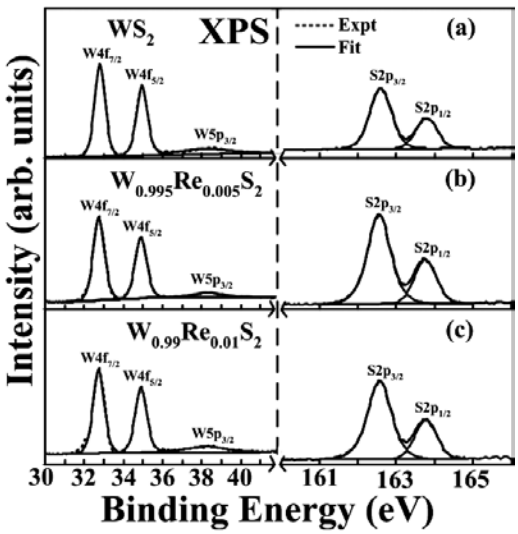

Figure 2. The XPS spectra in the vicinity of the W 4f and S 2p features for $W_{1-x}Re_xS_2$ single crystals (a) $x = 0$, (b) $x = 0.5\%$, and (c) $x = 1\%$.

used to calibrate the diffractometer. The lattice parameters were calculated with the aid of a computer using a least-squares refinement program.

Figure 1 shows the x-ray powder diffraction patterns for samples of nominal value x of 0.5% and 1%, respectively. The pattern of the undoped 2H-WS_2 single crystal is also included for comparison. The x-ray pattern of the Re-doped WS_2 crystals differs from that of the undoped WS_2 in that the relative intensities of the major lines are different, in addition to the presence of some extra lines (marked by *). The change in relative line intensities is most probably due to the presence of mixed 3R and 2H polytypes resulting in a different crystal quality. The additional lines were attributed to the presence of the rhombohedral polytype whose lattice parameters are $a = 3.149$ Å and $c = 18.434$ Å. It should be noted that the a lattice parameter is closed to the hexagonal polytype one ($a = 3.154$ Å) while the c lattice parameter is about 1.5 larger than the hexagonal polytype with $c = 12.362$ Å.

3.2. X-ray photoelectron spectroscopy

XPS spectra were recorded using a Thermo VG Scientific Theta Probe system under a base pressure of 10^{-9} Torr. Sample surfaces were cleaned under vacuum by argon ion etching until reproducible spectra were obtained. The Al Kα 1486.68 eV line was the x-ray source and the Ag $3d_{5/2}$ line at 368.26 eV was the calibration reference before measurement. Using Thermo VG Scientific (Avantage v1.68 software [15]), the accurate peak positions of the binding energy for $W_{1-x}Re_xS_2$ single crystals are determined by curve fitting using mixed Gaussian and Lorentzian line shape after the treatment of background by a Shirley function. Figures 2(a)–(c) are the slow scan XPS spectra in the vicinity of the W 4f and S 2p signals for the $W_{1-x}Re_xS_2$ ($x = 0$, 0.5% and 1%) single crystals, respectively. The line shape of the main structures (W $4f_{7/2,5/2}$ and S $2p_{3/2,1/2}$) of $W_{1-x}Re_xS_2$ shows no obvious difference. The W 4f doublet peak energies 32.75 eV (W $4f_{7/2}$) and 34.9 eV (W $4f_{5/2}$), and S 2p double peak energies 162.55 eV (S $2p_{3/2}$), and 163.8 eV (S $2p_{1/2}$) are identified in the spectra. Figures 3(a)–(c) depict the slow scan XPS spectra in the vicinity of the W 5p and Re 4f signals for the

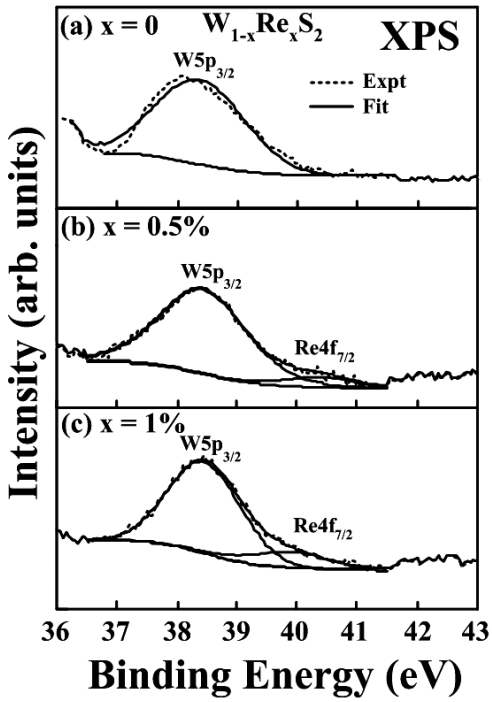

Figure 3. The XPS slow scan near the asymmetric W $5p_{3/2}$ feature for $W_{1-x}Re_xS_2$ single crystals (a) $x = 0$, (b) $x = 0.5\%$, and (c) $x = 1\%$. The weak shoulder on the higher energy side has been determined as the Re 4f feature.

$W_{1-x}Re_xS_2$ ($x = 0, 0.5\%$ and 1%) single crystals, respectively. As is shown in figure 3, the XPS spectra in the vicinity of the W 5p core-level range exhibit strongly asymmetric line-shape character. A weak shoulder located on the higher energy side is observed for the Re-doped samples (see figures 3(b) and (c)). The inclusion of the additional weaker feature is needed in order to have a reasonably good fit of the obtained spectra in the vicinity of the W $5p_{3/2}$ feature for the Re-doped samples. The peak positions determined are 38.45 ± 0.2 and 40.2 ± 0.2 eV, respectively, and they are assigned to originate from W $5p_{3/2}$ and Re $4f_{7/2}$. These results show evidence for the presence of Re in the doped samples. A qualitative comparison of the intensity of the Re 4f signal for the two doped samples showed that the nominal Re content with $x = 1\%$ is indeed larger than that of the $x = 0.5\%$ Re-doped sample.

3.3. Temperature-dependent electrical conductivity

The temperature dependence of the electrical conductivity was measured between 10 and 500 K by using a four-probe potentiometric technique. The selected samples were cut into a rectangular shape in the basal planes. The electrical contacts were made by mixing In–Ga alloy metal with silver paint. Electrical resistivity and Hall-effect measurements indicate that the doped samples are n-type in nature. At room temperature, the carrier concentration is $1–2 \times 10^{18}$ cm^{-3} and the Hall mobility is 20–30 cm^2 V^{-1} s^{-1}.

The conductivity of the doped samples is found to be much higher than that of the undoped one. This suggests that more charge carriers are available for conduction in the doped samples. From figure 4, the conductivity of the samples increases as the temperature is raised up to 500 K.

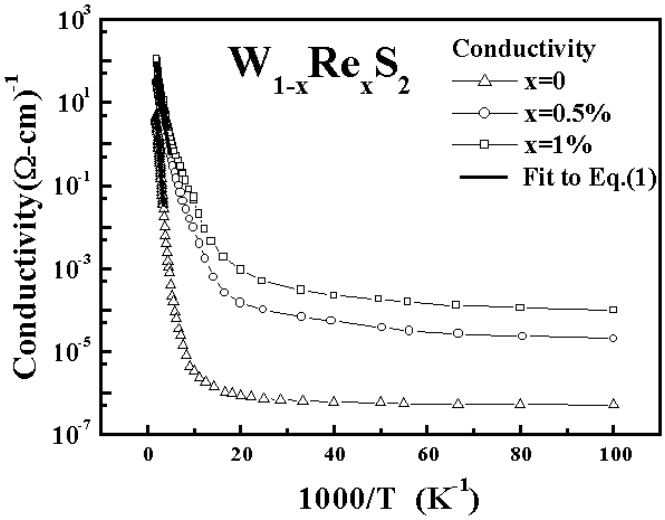

Figure 4. The temperature-dependent conductivity σ in the range 10–500 K for the $W_{1-x}Re_xS_2$ single crystals. The slopes of $\ln\sigma$ versus $1000/T$ yield carrier activation energies for the samples.

The temperature dependence of conductivity in the range of 250–500 K can be expressed as [16]

$$\sigma(T) = \sigma_0 \exp(-E_a/kT) \tag{1}$$

where E_a is the carrier activation energy. The $\ln\sigma$ versus $1000/T$ plots (figure 4) show the linear region where the slopes yield carrier activation energies for the samples. The activation energies of the doped samples $x = 0.5\%$ and 1% are determined to be 116 ± 5 meV and 113 ± 5 meV, respectively, which are much lower than that of the undoped one (299 ± 5 meV). These results together with the observation of higher conductivity reveal that the incorporation of Re into WS_2 has formed shallow impurity levels in the host crystals. This is in contrast to our previous observation for the Mo-doped ReS_2 crystals [17], that the incorporation of Mo into ReS_2 has formed deep impurity levels, resulting in a decrease in electrical conductivity.

3.4. Optical absorption

From the optical reflectivity and transmission measurements, the absorption coefficient α of the sample crystals can be determined by using the relation [18]

$$T_r = \frac{(1-R)^2 \exp(-\alpha d)}{1 - R^2 \exp(-2\alpha d)} \tag{2}$$

where T_r represents the transmission coefficient, R is the reflectivity and d the sample thickness. The variation of the absorption coefficient of Re-doped WS_2 and undoped WS_2 with photon energy is presented in figure 5. The non-uniform thickness and unsmooth sample surface will tend to cause the angles of incidence to deviate from the normal direction, resulting in some variations in the absorption spectra. Analysis of the experimental data on the absorption coefficient α shows an indirect allowed transition for the materials.

The experimental points for $(\alpha h\nu)^{1/2}$ versus photon energy, $h\nu$, that are deduced from absorption measurements for Re-doped and undoped WS_2 at 300 K are shown in figure 6, and

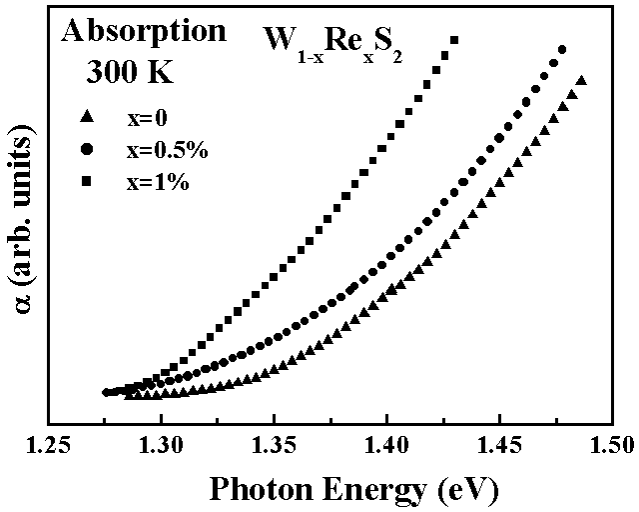

Figure 5. The variation of the absorption coefficient for the $W_{1-x}Re_xS_2$ single crystals with photon energy.

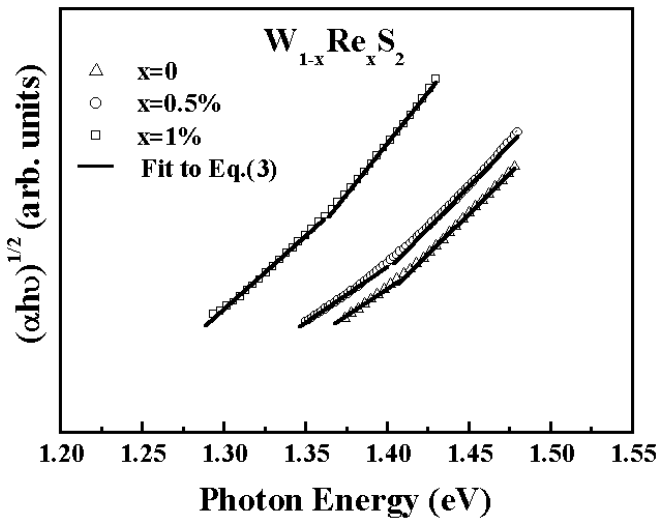

Figure 6. The experimental points of $(\alpha h\nu)^{1/2}$, deduced from absorption measurements, versus photon energy for the $W_{1-x}Re_xS_2$ single crystals. The solid curves are the least-squares fits to equation (3).

the solid curves are the least-squares fits to the expression [18]

$$\alpha h\nu = \frac{A(h\nu - E_g + E_p)^2}{\exp(E_p/kT) - 1} + \frac{B(h\nu - E_g - E_p)^2}{1 - \exp(-E_p/kT)} \tag{3}$$

where $h\nu$ is the energy of the incident photon, E_g the band gap, E_p the energy of the phonon assisting the transitions, and A and B are constants. The first term on the right-hand side of equation (3) corresponds to an absorption of a photon and a phonon, whereas the second term corresponds to an absorption of a photon and emission of a phonon and contributes only when $h\nu \geqslant E_g + E_p$. To evaluate the band gap E_g and phonon energy E_p with the use of equation (3),

Table 1. Summary of the results of optical absorption and PzR measurements for the $W_{1-x}Re_xS_2$ single crystals. Also included are the corresponding values of previous reports [19–21].

Materials	Indirect energy gap (eV) E_g	Phonon energy (meV) E_p	Excitonic transition energy (eV) E_A	E_B	Broadening parameter (meV) Γ_A	Γ_B
WS_2	1.29 ± 0.02[a]	27 ± 5[a]	1.984 ± 0.005[b]	2.394 ± 0.008[b]	31 ± 2[b]	57 ± 2[b]
$W_{0.995}Re_{0.005}S_2$	1.27 ± 0.02[a]	28 ± 5[a]	1.975 ± 0.005[b]	2.393 ± 0.008[b]	37 ± 2[b]	76 ± 2[b]
$W_{0.99}Re_{0.01}S_2$	1.24 ± 0.02[a]	22 ± 5[a]	1.948 ± 0.005[b]	2.346 ± 0.008[b]	53 ± 2[b]	92 ± 2[b]
WS_2[c]	1.3		1.95	2.36		
WS_2[d]	1.35		1.94	2.36		
WS_2[e]	1.3		2.0	2.386		

[a] This work (absorption).
[b] This work (piezoreflectance).
[c] [19] Thin film (absorption).
[d] [20] Thin film (absorption).
[e] [21] Thin film (absorption).

the background absorption is subtracted out. Differing values of E_g and E_p could be obtained by fitting a different energy range; thus errors of the order of ± 0.02 eV and ± 5 meV can be deduced for the estimates of E_g and E_p, respectively. The fitted values of the energy gaps and phonon energy of the sample crystals are summarized in table 1. For comparison, the values of the WS_2 energy gap of previous reports [19–21] are also included in table 1. The obtained value of 1.29 eV agrees well with Ballif *et al* [19] and Li *et al* [21]. The results show that the incorporation of a nominal 1% Re into WS_2 shifts the absorption edge about 0.05 eV towards the lower energy region. The shift for a nominal 0.5% Re is ~0.02 eV. The physical origin of the shift may come from the existence of n-type impurity, which in general will contribute to the absorption near the band tail. This red shift increases with the increase in the doping concentration.

3.5. Piezoreflectance

The direct band-edge excitonic transitions were studied at 300 K. Displayed in figure 7 are the PzR spectra in the range 1.9–2.5 eV at 300 K for undoped (top), 0.5% Re-doped (middle) and 1% Re-doped (bottom) WS_2 single crystals. The spectra are characterized by two prominent excitonic transitions, A and B. In the case of undoped WS_2, an adjacent antiresonance feature above the A exciton, denoted as A_R, is also detected. In order to determine the positions of the transitions accurately, we have performed a theoretical line shape fitting. The functional form used in the fitting procedure corresponds to a first derivative Lorentzian line shape function of the form [22]

$$\frac{\Delta R}{R} = \mathrm{Re} \sum_{j=1}^{m} C_j e^{i\phi_j} (h\nu - E_j + i\Gamma_j)^{-n} \tag{4}$$

where the subscript j refers to the type of interband transition, C_j and ϕ_j are the amplitude and phase of the line shape, E_j and Γ_j are the energy and broadening parameter of the transition, and the value of n depends on the origin of the transition. For the first derivative functional form, $n = 2.0$ is appropriate for the bounded states, such as excitons or impurity transitions [22]. Least-squares fits using equation (4) with $n = 2$ can be achieved, and the fits are shown as solid curves in figure 7. The fits yield the parameters E_j and Γ_j. The obtained values of E_j are indicated as arrows and denoted as A, B and A_R, respectively. The notation used here

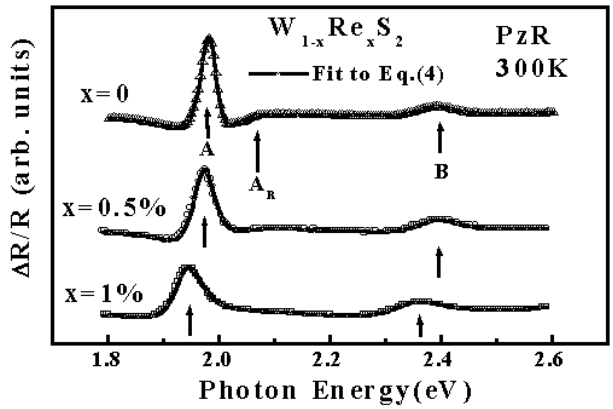

Figure 7. The PzR spectra of the $W_{1-x}Re_xS_2$ single crystals at 300 K. The solid curves are the least-squares fits using equation (4). Arrows under the curves show the peak positions of the two interband excitonic features, A and B, respectively. The antiresonance feature denoted A_R for WS_2 is also indicated.

follows closely that of Wilson and Yoffe [12] and Beal *et al* [23]. The obtained values of E_j and Γ_j are summarized in table 1. For comparison, the corresponding values for WS_2 of previous reports [19–21] are also listed in table 1. The values of E_j obtained for the undoped WS_2 show a general agreement with slight deviation from the corresponding room temperature transmission data of WS_2 [19–21]. We believe the derivative nature of the PzR spectra should offer better accuracy. As listed in table 1, the transition energies for excitons A and B show a slight red shift due to the presence of a small amount of Re. This red shift increases with increasing Re composition. In addition, the effect of the dopant is also clearly manifested in the increase of the broadening parameters Γ_A and Γ_B of the excitonic features A and B. The increase of the broadening parameter for the Re-doped samples is mainly due to impurity scattering.

4. Summary

In summary, single crystals of Re-doped WS_2 surface area up to 8×8 mm^2 and 1 mm in thickness have been grown by the chemical vapour transport method using bromine as a transport agent. The x-ray investigation indicates that the doped crystals are crystallized in mixed polytypes of the 3R and 2H structures. The AES and XPS spectra show evidence for the presence of Re in the doped samples. The presence of Re impurity has been determined to play a major role in influencing the electrical and optical properties of the doped samples. The electrical conductivity increases drastically with increasing Re concentration. The indirect energy gap determined from optical absorption measurements for the doped samples shows red shifts on increasing the doping concentration. The direct band edge excitonic transition energies show a slight red shift due to the presence of a small amount of Re, and the broadening parameter of the excitonic transition features increases due to impurity scattering.

Acknowledgments

The authors P C Yen and Y S Huang gratefully acknowledge the support of the National Science Council of Taiwan under Project no NSC92-2112-M011-001 and author K K Tiong

acknowledges the support by the National Science Council of Taiwan under the project no NSC92-2112-M019-008.

References

[1] Ouadah A, Pouzet J and Bernède J C 1993 *J. Physique* III **3** 1
[2] Tributsch H 1977 *Z. Naturf.* a **32** 972
[3] Li S J, Bernède J C, Pouzet J and Jamali M 1996 *J. Phys.: Condens. Matter* **8** 2291
[4] Jager-Waldau A, Lux-Steiner M, Jager-Waldau R, Burkhardt R and Bucher E 1990 *Thin Solid Films* **189** 339
[5] Fleischauer P D 1987 *Thin Solid Films* **154** 309
[6] Yanagisawa M 1993 *Wear* **168** 167
[7] Jager-Waldau A, Lux-Steiner M, Jager-Waldau G and Bucher E 1993 *Appl. Surf. Sci.* **70/71** 731
[8] Tributsch H 1979 *Solar Energy Mater.* **1** 257
[9] Tiong K K and Shou T S 2000 *J. Phys.: Condens. Matter* **12** 5043
[10] Christy R J 1980 *Thin Solid Films* **73** 299
[11] Traill R J 1963 *Can. Mineral.* **7** 524
[12] Wilson J A and Yoffe A D 1969 *Adv. Phys.* **18** 193
[13] Wildervanck J C and Jellinek F 1971 *J. Less-Common Met.* **24** 73
[14] Schroder D K 1998 *Semiconductor Material and Device Characterization* 2nd edn (New York: Wiley) chapter 10, p 671
[15] Thermo V G Scientific: Avantage Software, West Sussex, England
[16] Mahalaway S H and Evans B L 1977 *Phys. Status Solidi* b **79** 713
[17] Yen P C, Chen M J, Huang Y S, Ho C H and Tiong K K 2002 *J. Phys.: Condens. Matter* **14** 4737
[18] Pankove J I 1975 *Optical Processes in Semiconductors* (New York: Dover)
[19] Ballif C, Regula M, Regula P E, Remskar M, Sanjinés R and Lévy F 1996 *Appl. Phys.* A **62** 543
[20] Tonti D, Varsano F, Decker F, Ballif C, Regula M and Remskar M 1997 *J. Phys. Chem.* B **101** 2485
[21] Li S J, Bernède J C, Pouzet J and Jamali M 1996 *J. Phys.: Condens. Matter* **8** 2291
[22] Pollak F H and Shen H 1993 *Mater. Sci. Eng.* R **10** 275
[23] Beal A R, Knights J C and Liang W Y 1972 *J. Phys. C: Solid State Phys.* **5** 3540